

ATLAS 13 TeV Data Analysis using Particle Flow

Christian Kirfel

Bachelorarbeit in Physik

angefertigt im Physikalischen Institut

vorgelegt der

Mathematisch-Naturwissenschaftlichen Fakultät

der

Rheinischen Friedrich-Wilhelms-Universität

Bonn

November 2016

DRAFT

Ich versichere, dass ich diese Arbeit selbstständig verfasst und keine anderen als die angegebenen Quellen und Hilfsmittel benutzt sowie die Zitate kenntlich gemacht habe.

Bonn,
Datum
Unterschrift

1. Gutachter: Prof. Dr. Ian Brock
2. Gutachter: Prof. Dr. wildcard

Acknowledgements

I would like to thank ...

You should probably use \chapter* for acknowledgements at the beginning of a thesis and \chapter for the end.

DRAFT

DRAFT

Contents

1	Introduction	1
2	Theoretical and experimental basics	3
2.1	The Standard Model of Particle Physics	3
2.2	The LHC and ATLAS	5
2.2.1	The LHC	5
2.2.2	The ATLAS Detector	6
2.2.3	Tracking detectors	6
2.2.4	Calorimeter	8
3	Particle Flow Reconstruction	9
3.1	The Particle Flow Algorithm	9
3.1.1	Track selection	10
3.1.2	Clustering	10
3.1.3	Matching track to cluster	10
3.1.4	Cell Subtraction	10
3.1.5	Eflow Rec performance studies	11
3.1.6	Recent updates in eflowrec	12
4	Analysis framework	13
4.1	Trigger system	13
4.2	Event cleaning	13
4.3	Jet cleaning	13
4.4	The Good Run List	13
4.5	Jet Calibration and Smearing	13
4.6	The jet vertex tagger	14
4.7	Trigger Tools	14
4.8	Monte Carlo Re-weighting	15
4.9	Data Re-weighting	15
4.10	Muon Calibration and Selection	15
4.11	Electron Calibration and Selection	15
5	Results	19
5.1	The $Z \rightarrow \mu\mu$ decay	19
5.2	Event selection	19
5.3	Data/Monte Carlo comparison	19
A	Useful information	21

List of Figures	23
List of Tables	25

DRAFT

CHAPTER 1

Introduction

The Particle Flow algorithm is a promising approach of data analysis and has already been approved before on CMS as well as on ATLAS 2015 data. The combination of tracker and calorimeter information allows to improve the resolution especially in lower energy regions and can therefore reduce the energy threshold for analysis. The aim of my thesis was to create an analysis framework allowing Particle Flow analysis on 2016 13 TeV data and to show the improvements the new algorithm can yield. The second chapter of this thesis gives a brief introduction to the Standard Model of particle physics, the approved model used to describe most particle interactions, decays and crosssections. Furthermore the chapter includes a description of the ATLAS detector and its components and in addition a more general explanation of the attributes of tracking detectors and calorimeters to explain why better results are expected from the combination of both.

In the third chapter I describe the Particle Flow algorithm in detail and also present a brief overview of the Run 1 results as well as of the changes that have been applied to the algorithm since its first application in ATLAS.

Chapter four then summarizes the actual analysis framework that has been developed during my thesis. I give an explanation of all the important tools used in the framework and conclude by listing the difficulties and obstacles that still have to be overcome to complete a comprehensive analysis framework for Particle Flow.

Finally in chapter five I present the results derived from data/Monte Carlo comparison for 2016 data on $Z \rightarrow \mu\mu$ events.

CHAPTER 2

Theoretical and experimental basics

2.1 The Standard Model of Particle Physics

The Standard Model of particle physics summarizes the current knowledge of fundamental particles and their interactions. The model applies to scales of 1 fm and below. Gravity, being the fourth fundamental force is not included as it is negligible for most phenomena at this scale.

The current view is that all matter is made out of three kinds of elementary particle being leptons quarks and mediators. There are six leptons falling into three families according to their charge, electron number, muon number and tau number.

Similar to that there are six flavors of quarks separated by strangeness (S), charm (C), beauty (B), and truth (T). As the leptons the quarks fall into three generations. For both kinds of particles the mass rises with the generations and each generation comes as a doublet. The first particle of each lepton doublet is uncharged and referred to as a neutrino while the second particle has charge -1 . For each quark doublet there is an element with fractional charge $-\frac{1}{3}$ and an element with fractional charge $\frac{2}{3}$. To each of these particles exists an anti particle of opposite charge.

The third kind of particle included in the standard model is the mediator. Mediators are gauge bosons the exchange of which allows the particles to interact. There are four kinds of elementary interactions of which the strong electromagnetic and weak interaction are included in the model. The fourth interaction is the gravitational force. The gauge particles for the strong interaction are the gluons carrying colour charge, the electromagnetic mediator is the photon (γ) and the weak mediators are the W^\pm and Z bosons. Tables 2.1, 2.2 and 2.3 summarize the particles and their important properties.

Table 2.1: Lepton properties

	symbol	Charge	L_e	L_μ	L_τ
First generation {	e	-1	1	0	0
	ν_e	0	1	0	0
Second generation {	μ	-1	0	1	0
	ν_μ	0	0	1	0
Third generation {	τ	-1	0	0	1
	ν_τ	0	0	0	1

Table 2.2: Quark properties

	Symbol	Charge Q	mass	D	U	S	C	B	T
First generation {	d	$-\frac{1}{3}$	4.8 MeV	-1	0	0	0	0	0
	u	$\frac{2}{3}$	2.3 MeV	0	1	0	0	0	0
Second generation {	s	$-\frac{1}{3}$	95 MeV	0	0	-1	0	0	0
	c	$\frac{2}{3}$	1 275 MeV	0	0	0	1	0	0
Third generation {	b	$-\frac{1}{3}$	4 180 MeV	0	0	0	0	-1	0
	t	$\frac{2}{3}$	173 210 MeV	0	0	0	0	0	1

Table 2.3: Mediator properties

Interaction	Theory	Mediator	Charge	Coupling
Strong	QCD	gluons (8)	colour	1
Electromagnetic	QED	photon γ	electric charge	10^{-1}
Weak	GSW	W^\pm, Z	weak isospin	20^{-6}

Given this the standard model of particle physics has been a very successful model for a very long time and still holds for most cases. Nevertheless the model has some commonly known weaknesses and does not claim to be complete. For example the gravitational force is not included and in the standard model neutrinos are massless which would not allow the oscillations observed in neutrinos originating from the sun. For further information check [**griffith08**], [**thomson13**] and [**brock11**].

There should be a short sentence about the Higgs Boson but I am unsure what to write exactly ?

2.2 The LHC and ATLAS

The analysis for this thesis has been performed in the ATLAS collaboration. The ATLAS-Detector is one of the four main experiments at the LHC at Cern. Therefore this chapter provides a brief overview over the LHC and ATLAS focusing on the properties directly relevant for Particle Flow Analysis.

After a description of the ATLAS detector in general I will give some further information about the detector components directly relevant for the explanation of particle flow which are the tracking detector and the calorimeter. To make the advantages of particle flow understandable to the reader I will give a general description of these detectors and their properties irrespective of their detailed construction at ATLAS.

2.2.1 The LHC

The Large Hadron Collider ("LHC") is part of the facilities of the European Organization of Nuclear Research ("CERN") and was built to extend the frontiers of modern particle physics by delivering high luminosities and unprecedented high energies. The Collider is circular with a circumference of 26.659 km and is located 10 km underground close to Geneva.

The LHC is designed to collide bunches of up to 10^{11} protons at a luminosity of $10^{34} \text{ cm}^{-2} \text{ s}^{-1}$. The beams are collided at four collision points representing the four main experiments at the LHC. Two of these are special-purpose detectors, namely LHCb and ALICE while the other two are general-purpose detectors. The general-purpose experiments are CMS and ATLAS. The analysis in this thesis was performed on ATLAS data. Figure 2.1 shows the LHC, the four detectors and its general location.

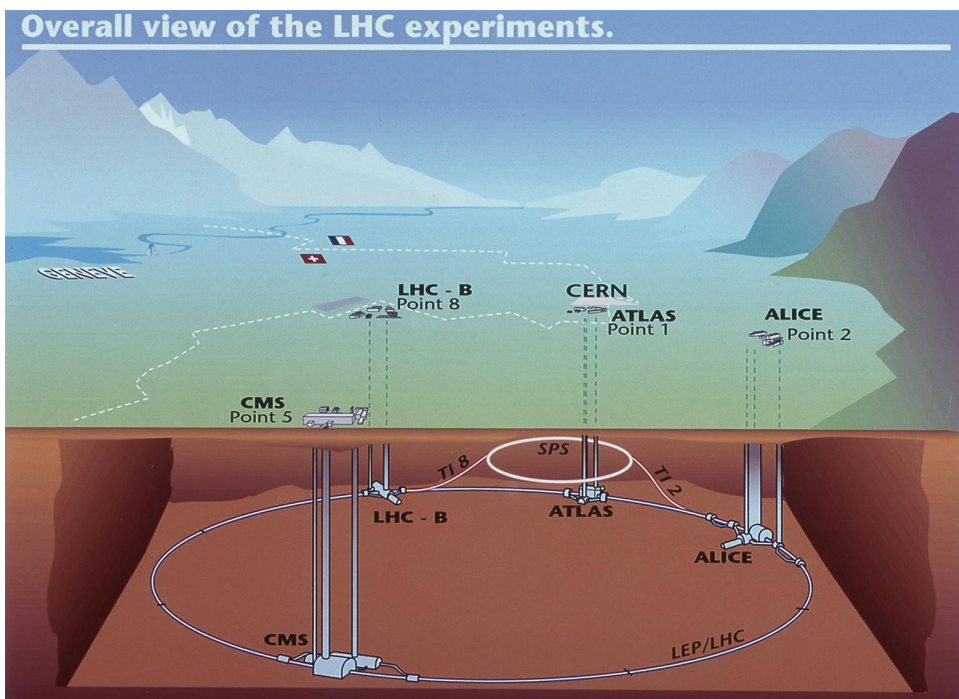


Figure 2.1: Sketch of the LHC ring, the position of the experiments and the surrounding countryside. The four big LHC experiments are indicated(ATLAS, CMS, LHC-B and ALICE)along with their injection lines(Point 1, 2, 4, 8)[[atlasfigures](#)]

2.2.2 The ATLAS Detector

The ATLAS-Detector was developed to take advantage of the high energy available at the LHC enabling the observation of highly massive particles that lower energy accelerators were not able to create and that way bring new physics theory beyond the standard model of particle physics. It is designed to be able to observe a maximized number of final stages being a so called general purpose-detector. This means that the detector should be able to identify all kinds of particles and still provides an accurate information about angle and momentum. Figure 2.2 shows the outline of the ATLAS detector together with a rough scale in size. In the following explanations of its components are given from the inside to the outside.

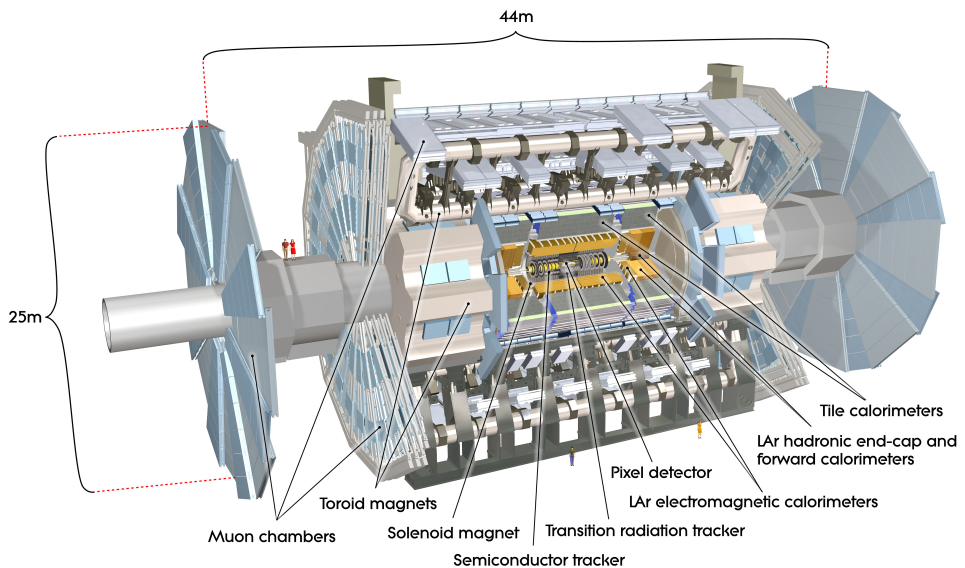


Figure 2.2: Sketch of the ATLAS detector [[atlasfigures](#)]

Figure 2.3 shows the detector's components in a simplified way and allows to understand the order of the important detector parts in detail. The innermost part of the detector is a tracking detector in a field of a large solenoid coil to obtain charge and trajectory of charged particles. The following two parts are the electromagnetic and hadronic calorimeter which together build the calorimeter part of the detector. One of them focuses on measuring the energy in electromagnetic showers while the other one is optimized for hadronic particle showers. The outermost part is a muon spectrometer because most of the particles that cross the calorimeters undetected are muons.

2.2.3 Tracking detectors

The go to method to measure the momenta of charged particles is based on tracking detectors, which detect and monitor charged particles leaving behind tracks of ionizations in any given medium allowing to reconstruct the particle's trajectories. There are two main categories of tracking detectors. The first one uses a large gaseous volume in a strong electric field and is filled with an area of wires. The electric field makes the liberating electrons drift towards the wires where they cause a detectable signal.

The second type of detectors is based on semiconductor technology and is used in most modern detectors like ATLAS. Therefore I will describe this kind of tracking detectors in more detail. If a charged particle traverses an appropriately doped semiconductor wafer for example a doped silicon wafer

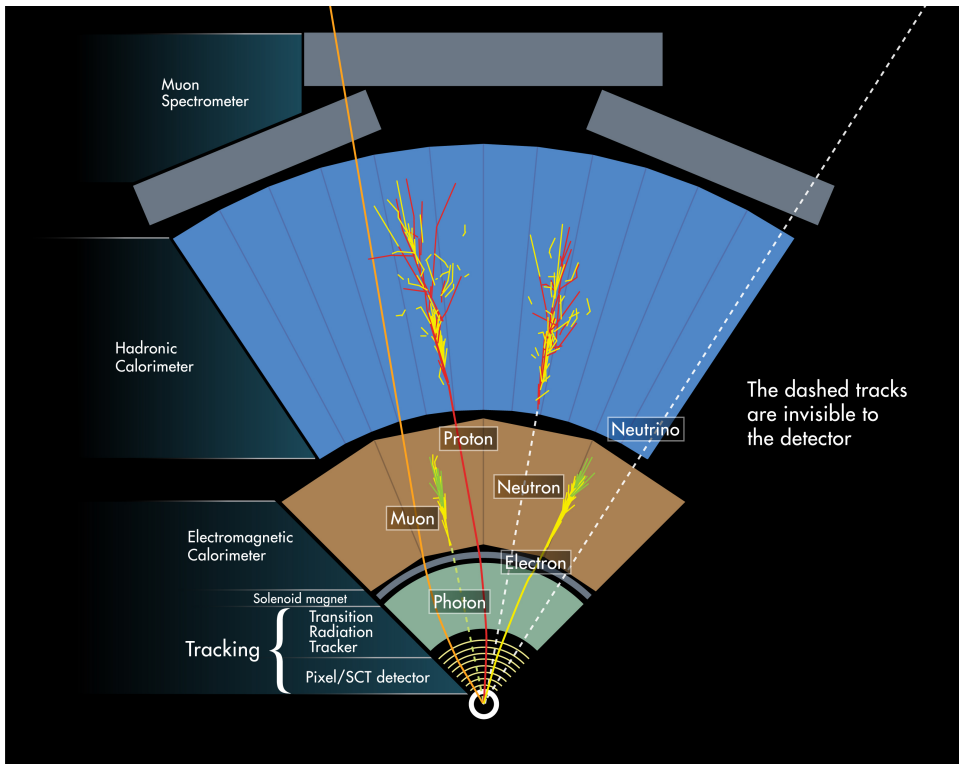


Figure 2.3: Scheme of the ATLAS-detector [atlasfigures]

it creates electron hole pairs along its trail. If an electric field is applied to the semiconductor material the holes will drift in the direction of the electric field and can then be collected by p-n junctions.

Usually a tracking detector is structured into semiconductor strips or pixel with a magnitude of $25\text{ }\mu\text{m}$, which allows to precisely determine the position of the event. By relating a set of events to a single particle and knowing the space and time of these one can then extrapolate the track from the triggered pixels. The common way of setting up such a tracking detector is an array of cylindrical semiconductor wafers in a magnetic field. Each wafer signal gives a rough estimation of the particle's location at the time and the curve given by the sum of signals allows to calculate its charge and momentum.

$$p \cdot \cos\lambda = 0.3BR \quad (2.1)$$

Inner Detector

The Tracking detectors of the ATLAS detector are called the Inner Detector, which consists of three sub-components, the Pixel detector (Pixel), the Semi-Conductor Tracker (SCT) and a Transition Radiation Tracker (TRT). Each of these sub-detectors is divided into the so called barrel part and two end-caps. The Inner Detector covers a region of $|\eta| < 2.5$ which also limits the region in which Particle Flow can be used.

Muon spectrometer

The outermost part of the detector is formed by the muon tracking chambers, the so called muon spectrometer. The task of the spectrometer is to detect charged particles transversing the calorimeter

undetected and to both trigger on them and to measure their energy. Due to these two functions the spectrometer is divided into two parts each dedicated to one of the tasks. The first part is the trigger chamber covering a range of $|\eta| < 2.4$, followed by the high-precision chamber with a range of $|\eta| < 2.7$. The main detector's support feet cause a further gap at about $\phi = 300^\circ$ and $\phi = 270^\circ$.

The high-precision detector uses monitored drift tubes (MDTs) while the trigger chamber uses resistive-plate chambers (RPCs). The momentum calculation is then performed by the field of the torroid magnet.

2.2.4 Calorimeter

In particle physics a calorimeter is a device to measure first and foremost the total energy of a particle. Most of the time additionally some positional information is taken. The idea is that most particles loose all their momentum crossing the calorimeter-structure. Measuring the energy deposited this way gives a value for the particle's energy. Usually a particle deposits its energy by initiating a particle shower, the energy of which is then collected and measured. Calorimeters are distinguished by the main interaction of the particles one aims to detect.

Electromagnetic Calorimeter

Electromagnetic calorimeters are designed to detect charged particles and measure their total energy. Usually these particles are electrons and photons. There are various methods to construct these detectors. An example would be the usage of inorganic scintillators. These scintillators should be optically transparent and have a short radiation length to contain the shower in a compact region. The detection can then be followed by photon detectors which measure the emitted light being proportional to the detected particle's energy. The energy resolution of these detectors is typically in the range of

$$\frac{\sigma_E}{E} \sim \frac{3\% - 10\%}{\sqrt{E/\text{GeV}}}. \quad (2.2)$$

The electromagnetic calorimeter at ATLAS is a high-resolution and high-granularity liquid-argon sampling calorimeter with lead as absorber material. The calorimeter consists of two half-barrels which are only separated by a small gap at the interaction point. The endcaps at each side are segmented into two coaxial wheels to cover different polar angles.

Hadronic calorimeters

Hadronic calorimeters are used to obtain the energies of hadronic particle showers. Due to the relatively large distance between interactions these calorimeters occupy a significantly large volume in the detector.

A common technique to construct these calorimeters is a sandwich-like structure of alternating layers of high density absorber material and active material. The absorbers are used to develop the particle showers which then hit the active material and deposit their energy there. That way hadronic calorimeters reach a resolution of about

$$\frac{\sigma_E}{E} \gtrsim \frac{50\%}{\sqrt{E/\text{GeV}}} \quad (2.3)$$

which is about one order of magnitude worse than for an electromagnetic calorimeter.

The hadronic calorimeters at ATLAS are.... For more information see the ATLAS design report [\[atlastdr\]](#)

CHAPTER 3

Particle Flow Reconstruction

One of the goals of this thesis was to check the results of Particle Flow in Run 2 data. Therefore this chapter will give an overview of the results that the new algorithm has brought for Run 1 in data MC comparison. Before showing the results this chapter gives a description of the algorithm based on the Particle Flow Paper [[pflow16](#)]. Then an update on how the algorithm has evolved is given before finally a brief overview of the results is presented.

3.1 The Particle Flow Algorithm

Recently only either the Calorimeter or the tracker information was used to reconstruct Jets in ATLAS events. The Particle Flow algorithm now combines tracker and calorimeter information to achieve better resolution especially at lower energies. The main advantages of including the tracker information into reconstruction are as follows:

- For low energy charged particles the momentum resolution of the tracking detector is superior to the calorimeter.
- The tracking detector is able to reconstruct soft particles, which would not pass the noise threshold of the calorimeter.
- The ATLAS tracking detector has a superior angular resolution for single charged particles.
- Low p_T charged particles may be swept out of the cone before reaching the calorimeter by the magnetic field. The tracker information allows to cluster these particles into the jet.
- a better vertex determination could lower the pileup-contribution.

The advantages of Particle Flow have already been shown for Run 1 data in

Figure 3.1 sketches the important steps of the Particle Flow algorithm. The algorithm uses clusters from the calorimeters and tracks from the tracking detectors as input information. The first step is to match a track spatially to a cluster. After a pair has been found the algorithm checks whether the particle's momentum matches the energy deposited in the cluster within the expected deviation. If the energy matches a subtraction algorithm starts deciding which cells belong to the given event. If the energy deposited in the cluster is too low the algorithm includes all other clusters in a given area and then starts the subtraction.

After the subtraction the algorithm gives information about matched clusters and trackers. Furthermore energy deposited in cells that were not subtracted can be identified as remnants.

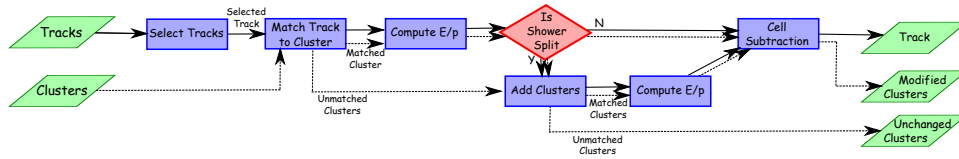


Figure 3.1: Flowchart of the steps of the Particle Flow algorithm [pflow16]

3.1.1 Track selection

In spite of the clusters the algorithm has some requirements on tracks to be selected to minimize the amount of fake tracks. The requirements are at least 9 hits in the PIXEL and SCT and no missing hits in the PIXEL at all. The tracks have to be in a pseudo-rapidity region of $|\eta| < 2.5$ and $500 \text{ MeV} < p_T < 40 \text{ GeV}$.

3.1.2 Clustering

The algorithm uses given information from the tracker and the calorimeter as input. The information from the calorimeter is give as topological clusters. The construction of these clusters is briefly described in this chapter to give the reader a basic understanding which input information the algorithm uses.

Each cluster is being constructed around a so called seed cell. A seed cell is a cell for which the deposited energy exceeds the expected noise by four times the standard deviation. If a seed is found all the neighboring cells which exceed the noise by at least two times the standard deviation are added to the cluster. Finally all the cells neighboring these clusters are also added.

3.1.3 Matching track to cluster

The algorithm tries to match every track to one or more calorimeter clusters. First the algorithm tries to match a single best-match topo-cluster to every selected track. To do so the distances in $\Delta\phi$ and $\Delta\eta$ from the track are extrapolated to the second layer of the EM calorimeter and the topo-clusters. After that the topo-clusters get ranked based on the metric:

$$\Delta R' = \sqrt{\left(\frac{\Delta\phi}{\sigma_\phi}\right)^2 + \left(\frac{\Delta\eta}{\sigma_\eta}\right)^2} \quad (3.1)$$

where σ_η and σ_ϕ refer to the angular topo-cluster width, computed from the standard deviation of the displacemtens of the topo clusters. If the energy in this cluster is greater than or equal to the energy estimated from the track's p_T the algorithm goes to cell subtraction. If the energy in the cluster is smaller than the expected enegery all clusters in a cone of $\Delta R < 0.2$ are matched to the track. In that case R is calculated by the metric:

$$\Delta R = \sqrt{(\Delta\phi)^2 + (\Delta\eta)^2} \quad (3.2)$$

3.1.4 Cell Subtraction

The last step in the Particle Flow algorithm after matching a set of topo-clusters to a track is the cell-wise subtraction of energy deposits to remove remnants and determine which energy depositions belong to the given particle. If the energy deposited in the set of clusters falls below the expected energy the clusters are simply removed. Otherwise, a cell by cell subtraction is performed.

The first step of the cell subtraction is generating a shower shape from the extrapolated track. Around the extrapolated track rings in η, ϕ space are generated just wide enough to independently contain at least one cell from the extrapolated position. Furthermore the rings are restricted to one layer and of the same radial size for each layer. After the generation of rings in each layer the average energy density in each ring is computed and the rings are ranked by energy density in descending order. The layer is not used in any way for this ranking. The subtraction then starts from the ring with highest energy density and proceeds successively to rings of lower order until the next ring's energy exceeds the remaining expected energy. If the ring's energy exceeds the energy still to be subtracted the energy in each cell is scaled down by the fraction needed to reach the expected energy before the process halts and the remaining cells are removed as remnants. An example of the process is sketched in figure 3.2.

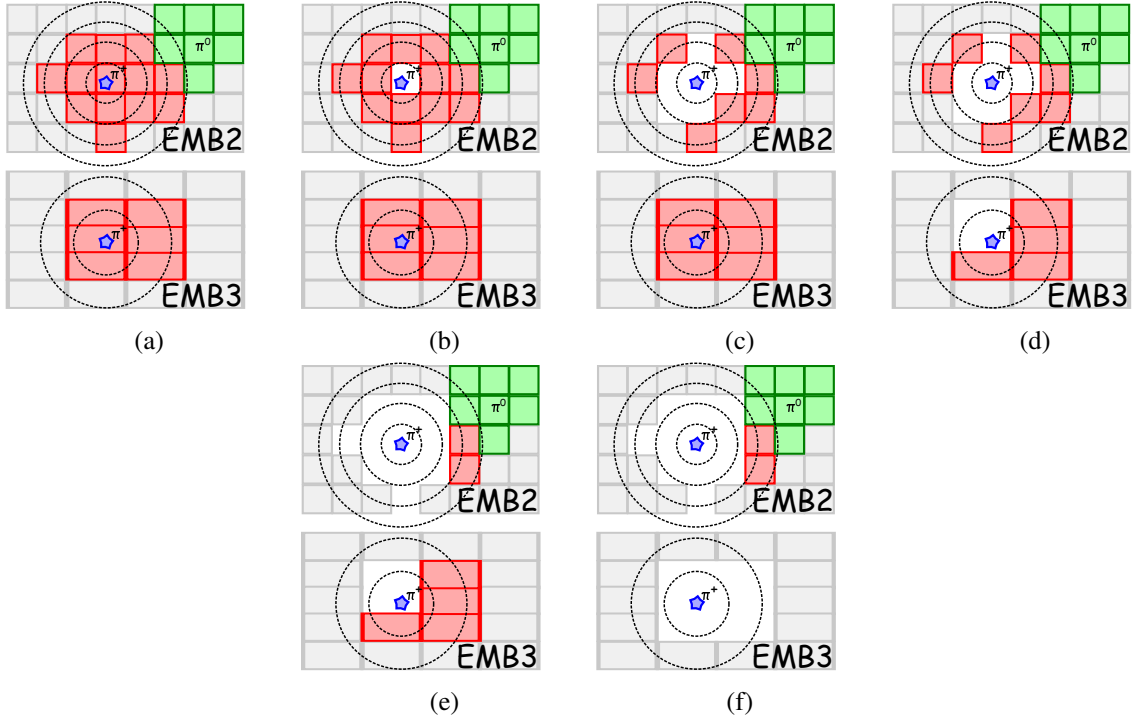


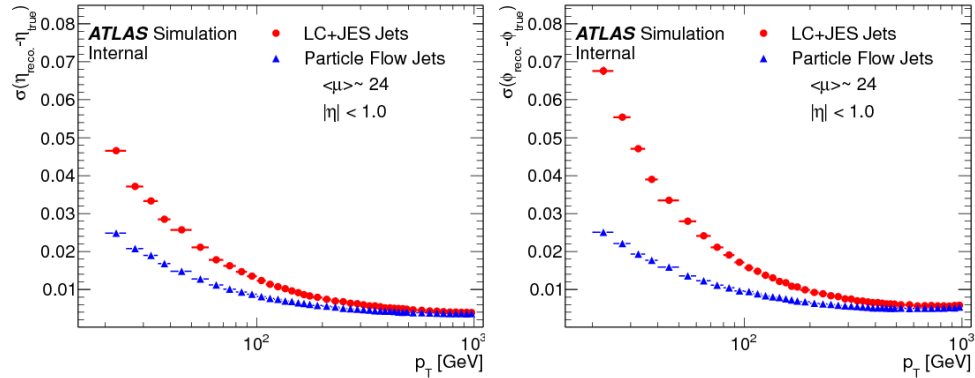
Figure 3.2: Example of cell subtraction. In red the depositions originating from the π^+ of interest are shown and in green a cluster from a π^0 are shown. [pflow16]

3.1.5 Eflow Rec performance studies

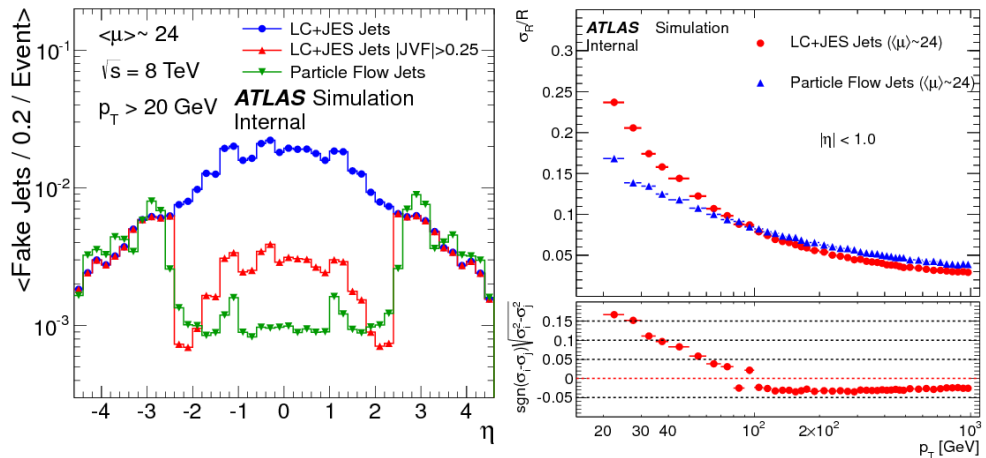
The Particle Flow manuscript shows the impact of the new algorithm on the angular resolution and on the rejection of pileup jets. This section briefly summarizes the important results of this study. Figure 3.3(a) and 3.3(b) show the improvements in angular resolution while figure 3.4(a) displays the increased rejection of fake jets for the new algorithm. LC+JES jets are the jets using the old algorithm and JVF in figure 3.4(a) refers to the Jet Vertex Fraction representing the amount of energy in the jet originating from the original vertex.

The plots clearly demonstrate that Particle Flow does improve the angular resolution in low p_T regions while having no drawback for higher p_T regions. The pileup contribution is also mediated massively even in comparison to the usage of a cut on the JVT. The region of effect is restricted to $|\eta| < 2.5$ because only this region of pseudorapidity is covered by the Inner Detector. Only the momentum resolution shown in

figure 3.4(b) worsens using the old reconstruction for high p_T regions.



(a) Improvements in η resolution for Particle Flow Jets [pflow16] (b) Improvements in ϕ resolution for Particle Flow Jets [pflow16]



(a) Pileup comparison of EM-Topo Jets and Particle Flow jets [pflow16] (b) Momentum resolution of Particle Flow jets [pflow16]

3.1.6 Recent updates in eflowrec

The description of the Particle Flow algorithm given in this thesis is based on the analysis of Run 1 data and some recent changes to the algorithm are described in this section.

CHAPTER 4

Analysis framework

In order to construct a framework for general Particle Flow analysis and data Monte Carlo comparison a large amount of ingredients is needed to be included and checked to be correctly working. In this chapter I will go over the important tools included in my framework. The impact of every given tool will be demonstrated and possible problems in current implementation are also included to summarize the status of the framework. The description starts with the trigger system. The second section describes the general event selection tool and finally the calibrations for specific particles are introduced.

4.1 Trigger system

4.2 Event cleaning

4.3 Jet cleaning

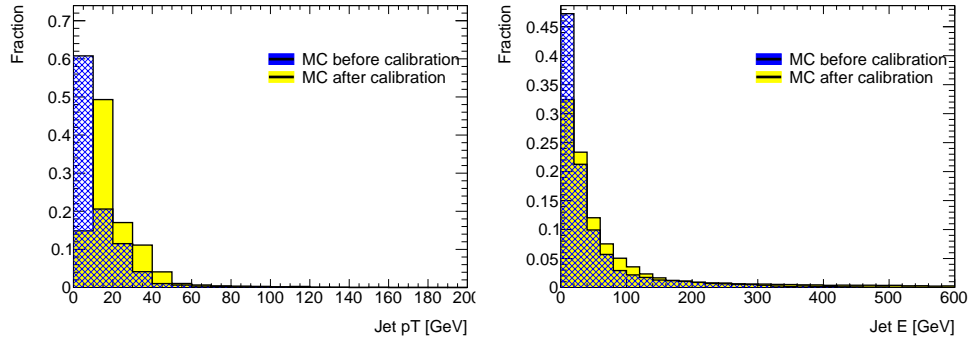
The Jet cleaning allows to apply certain requirements on jets in an event and therefore to remove jets or even complete events that might be bad data. The Jet Cleaning is used on both data and Monte Carlo to make sure that Monte Carlo events that would be removed in data also are not included in the simulation. Bad jets are excluded on the base of their wildcard. For this framework a wildcard selection has been chosen and if one bad jet is found the whole event is removed.

4.4 The Good Run List

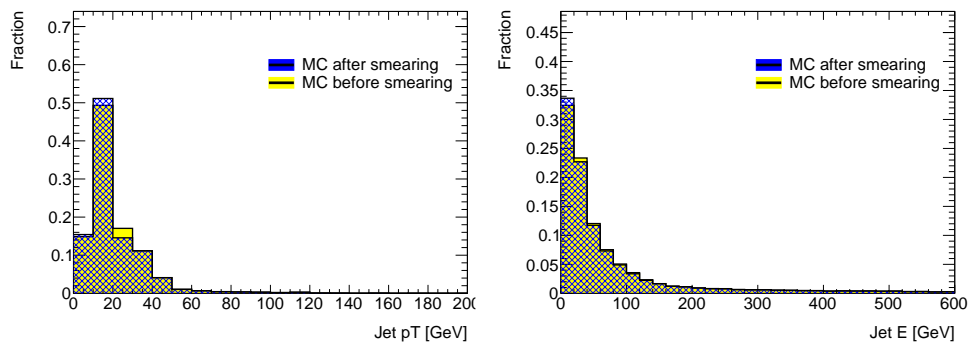
The Good Run List is only needed for actual detector data. For data to be suitable for analysis one has to make sure that it fits certain requirements of which some depend on the detectors working state. The Good Run List allows to exclude data-taking periods in which the detector showed a poor working state. Reasons for this may be maintenance on sub detectors, magnets off or ramping or an unstable beam of the LHC. The Good Run List includes all the good data taking periods and the tool excludes all data from bad periods. For the data analysis in this thesis the GRL wildcard is used.

4.5 Jet Calibration and Smearing

After making sure a jet is "good" and therefore has passed the cleaning it must still be calibrated and in case of MC smeared to data. The Calibration scales the energy of jets for a certain reconstruction



(a) The influence of the calibration in momentum is shown (b) The influence of the calibration in energy is shown



(a) The influence of the Smearing in momentum is shown (b) The influence of the Smearing in energy is shown

algorithm. The Smearing smears the MC resolution to be matching the actual data resolution.

4.6 The jet vertex tagger

Due to the high luminosity at the LHC in time and in space pileup is a big problem in ATLAS analysis. Therefor the rejection of pileup is an important part of analysis. One possible way to minimize pileup is to calculate the jet-vertex fraction of each jet which is the fraction of momentum in the jet originating from the primary vertex. If one sets a minimum on this fraction pileup can be suppressed because jets that do not pass the criteria on their JVF are highly likely to be originating from pileup vertices. The Jet Vertex Tagger relates each jet to a vertex.

4.7 Trigger Tools

A further important collection of tools has to make sure that the trigger is fired, correctly used and also that the particle that triggered is actually one of those used in later analysis.

A trigger basically is a first selection for an event meaning that an event is required to surpass certain demands to be used in analysis. These demands are embodied by so called trigger chains that can be used as input for a trigger tool in analysis which on that base can select or refuse events. For the analysis in this thesis the recommended single lepton triggers fpr 2016 data were used. THe chains were wildcard.

Usually the trigger is checked before the event is further cleaned and calibrated. Therefore it can happen that the particles that passed the trigger later get removed in the analysis. The trigger matching makes sure that the particles that passed the triggers are still left in the final analysis and if not the event can still be removed.

4.8 Monte Carlo Re-weighting

The Monte Carlo is produced before data is taken therefore the shape of Monte Carlo may vary from the shape of the actual taken data for several reasons. For example the pileup in MC may not match the data as well as the resolution. To compensate these differences a sum of weights is applied to Monte Carlo.

4.9 Data Re-weighting

4.10 Muon Calibration and Selection

Analog to jets the muons in an event also have to go through several cuts and have to be calibrated properly. This section introduces all the important tools for muon calibration and gives a brief summary of the effects of the cuts and calibrations. The first and foremost task of the muon tools is to determine whether a muon originated from the original vertex or has its origin in background noise(cosmic muons) or in some kind of secondary interaction. Muons are reconstructed using both the muon spectrometers and the inner detector. The information from both detector systems is combined to a single track. Then the muons are requested to have $p_T > 25 \text{ GeV}$ and a pseudorapidity of $|\eta| < 2.5$. To reject the cosmic muon background further the muons are not allowed to have a longitudinal impact parameter to the primary vertex that is higher than 3 mm. The last requirement is added due to muons originating from heavy flavour quark decays.

To remove these last unwanted muons an isolation criteria is implemented, namely the isolation tool. The tool makes sure that the sum of transversal momentum of the tracks around the muon candidate divided by the muons momentum is smaller than 0.05.

$$\frac{\sum_{\Delta R} pT_{track}}{muon p_T} < 0.05 \quad (4.1)$$

This way in $Z \rightarrow \mu^+ \mu^-$ events an efficiency of 97 % in muon detection was achieved.

The second part of the muon tools makes sure that the muon properties are correctly calibrated and smeared to make Monte Carlo and data match properly and to eliminate known weaknesses in the detector structure. Figure 4.3 shows the muons transversal momentum before and after calibration in Monte Carlo. The changes are very minor.

4.11 Electron Calibration and Selection

The electron tools are the more or the less parallel to the muon tools. There is a first group of tools and criteria to determine which electrons actually originate from the primary vertex and distinguishes those electrons from background and pileup. The second group of tools calibrates the wanted electrons properties.

Electrons are detected by leaving a track in the inner detector and depositing most of their energy in the electromagnetic calorimeter. The reconstruction algorithm expects a calorimeter cluster with a

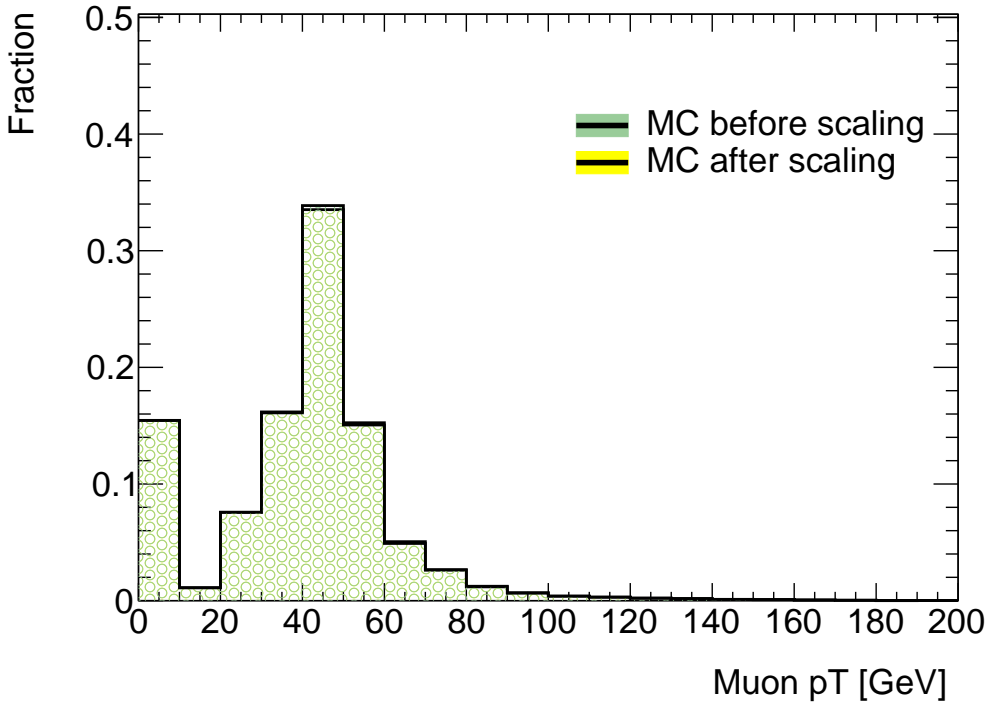


Figure 4.3: Calibration and smearing of the muon momentum. The changes are very minimal.

deposited energy E_T exceeding 2.5 GeV. This cluster has then to have a matching track from the primary hard scatter vertex. The η requirements are $|\eta|_{cluster} < 2.47$ with an exclusion of $1.37 < |\eta| < 1.52$ (calorimeter barrel-endcap transition region).

Electrons are same as muons required to be isolated. The Isolation is based on a $\Delta R < 0.2$ cone in the deposited energy and a $\Delta R < 0.3$ cone around the track.

The electron calibration and smearing is exemplary displayed in figure 4.4. The impact of the scaling is significantly higher than for muons.

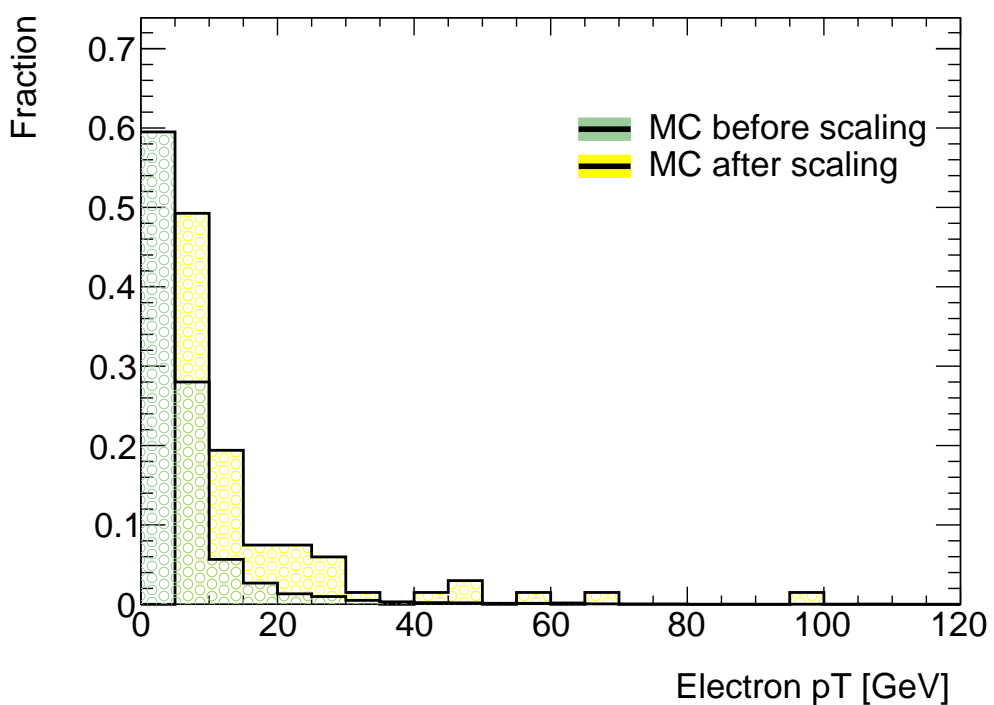


Figure 4.4: Calibration and smearing of the electron momentum.

CHAPTER 5

Results

5.1 The $Z \rightarrow \mu\mu$ decay

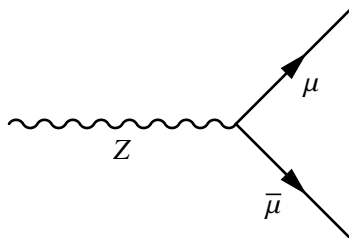


Figure 5.1: Decay of a Z-Boson to two muons

For this thesis $Z \rightarrow \mu\mu$ events were used. The decay channel of a Z boson into a muon and an antimuon has a cross-section of 3.366 ± 0.007 [pdg]. The event was chosen for this analysis because the Z boson is very easy to trigger on and it allows a very clear event selection. Furthermore the event has exactly one recoiling jet that analysis can be performed on.

5.2 Event selection

The criteria for the event selection were no good electrons and exactly two good muons, with opposite charge where good means that the particle passed all selection filters itself. The reconstructed Z-Boson is required to be in a range of (90 ± 10) GeV and to have a transversal momentum greater than 30 GeV while the muons are required to have a transversal momentum greater than 25 GeV. Furthermore the muons are restricted to a central η region being $|\eta| < 2.4$.

Furthermore a jet is required to have a transversal momentum greater than 20 GeV and is required to be recoiling to the reconstructed Z giving the selection criteria $|\phi_{jet} - \phi_Z| < (\pi - 0.4)$.

5.3 Data/Monte Carlo comparison

I know nothing

APPENDIX A

Useful information

In the appendix you usually include extra information that should be documented in your thesis, but not interrupt the flow.

List of Figures

2.1	Sketch of the LHC ring, the position of the experiments and the surrounding countryside.	5
2.2	Sketch of the ATLAS detector	6
2.3	Sketch of the transversal section of the ATLAS detector	7
3.1	Flowchart of the steps of the Particle Flow algorithm	10
3.2	Example of cell subtraction. In red the depositions originating from the π^+ of interest are shown and in green a cluster from a π^0 are shown. [pflow16]	11
4.3	Calibration and smearing of the muon momentum. The changes are very minimal.	16
4.4	Calibration and smearing of the electron momentum.	17
5.1	Decay of a Z-Boson to two muons	19

List of Tables

2.1	Lepton properties	4
2.2	Quark properties	4
2.3	Mediator properties	4